

## Article

# Synthesis of MRGO@ZIF-7-Based Molecular Imprinted Polymer by Surface Polymerization for the Fast and Selective Removal of Phenolic Endocrine-Disrupting Chemicals from Aqueous Environments

Ying Li <sup>1,2,\*</sup> , Yang Li <sup>1,2</sup>, Zhu Ding <sup>1,2</sup>, Dong Wan <sup>1,2</sup>, Zhong Gao <sup>1,2</sup>, Yu Sun <sup>1,2</sup> and Ying Liu <sup>3,\*</sup><sup>1</sup> School of Chemical Engineering and Technology, Tiangong University, Tianjin 300387, China<sup>2</sup> State Key Laboratory of Separation Membranes and Membrane Processes, Tiangong University, Tianjin 300387, China<sup>3</sup> School of Environmental Science and Engineering, Tiangong University, Tianjin 300387, China

\* Correspondence: ly@tiangong.edu.cn (Y.L.); ly9423@163.com (Y.L.)

**Abstract:** In this study,  $Zn(NO_3)_2 \cdot 6H_2O$  was selected as the metal source, and ZIF-7-modified magnetic graphene-based matrix materials (MRGO@ZIF-7) were prepared by in situ growth. ZIF-7 modified magnetic graphene-based molecular imprinting complexes (MRGO@ZIF7-MIP) were successfully synthesized by a surface molecular imprinting technique using bisphenol A (BPA) as the template molecule. The obtained experimental materials were characterized by X-ray diffraction (XRD), Brunner–Emmet–Teller (BET) analysis, scanning electron microscopy (SEM), transmission electron microscopy (TEM), vibrating sample magnetometry (VSM), and X-ray photoelectron spectroscopy (XPS). The proper adsorption and selective recognition ability of the MRGO@ZIF7-MIP were studied by an equilibrium adsorption method. The obtained MRGO@ZIF7-MIP showed significant molecular recognition of bisphenol A (BPA) and good selectivity and reproducibility for BPA in different aqueous environments such as drinking water, river water, and lake water. These properties make this material potentially applicable for the efficient removal of phenolic endocrine disruptors in real water environments.

**Keywords:** endocrine disrupting chemicals; molecular imprinting; ZIFs; magnetic graphene

**Citation:** Li, Y.; Li, Y.; Ding, Z.; Wan, D.; Gao, Z.; Sun, Y.; Liu, Y. Synthesis of MRGO@ZIF-7-Based Molecular Imprinted Polymer by Surface Polymerization for the Fast and Selective Removal of Phenolic Endocrine-Disrupting Chemicals from Aqueous Environments.

*Processes* **2023**, *11*, 1000. <https://doi.org/10.3390/pr11041000>

Academic Editors: Zhaoyang Wang, Hao Xu and Yan Feng

Received: 16 February 2023

Revised: 15 March 2023

Accepted: 23 March 2023

Published: 25 March 2023



**Copyright:** © 2023 by the authors. Licensee MDPI, Basel, Switzerland. This article is an open access article distributed under the terms and conditions of the Creative Commons Attribution (CC BY) license (<https://creativecommons.org/licenses/by/4.0/>).

## 1. Introduction

Phenolic endocrine-disrupting chemicals (PEDCs) in the aqueous environment have become an increasingly serious problem due to the widespread use of fine phenolic chemicals, pesticides, preservatives, and antioxidants in industrial and agricultural production [1,2]. PEDCs mainly consist of alkyl phenols, bisphenols, and chlorophenols, and they possess a common phenolic moiety that is responsible for their estrogenic activity. Alkyl phenols are usually the main raw material for the synthesis of nonionic surfactants and lubricant additives [3]. Bisphenols are a major member of the PEDCs, which contain two hydroxyphenyl groups in their structure and are widely used in the synthesis of various polymer materials, such as epoxy resins and polysulfone resins [4]. Chlorophenols are widely found in industrial wastewater produced by synthetic pesticides and the paper industry [5]. In daily life, they can enter the human body through drinking water, food, skin contact, and breathing [6,7]. If exposed for a long time, their environmental persistence, bioaccumulation, high toxicity and estrogenic activity can interfere with the human endocrine system, immune system, and reproductive system, leading to cardiovascular diseases, liver diseases, urinary system diseases, and human fertility diseases, as well as serious harm to the ecological environment and human health [8–10].

The current removal methods of PEDCs in the water environment can be divided into three categories: physical methods, chemical methods, and biological methods,

among which physical methods mainly include activated carbon adsorption and membrane filtration [11]; chemical methods mainly include ozonation, chlorine oxidation, and UV/hydrogen peroxide oxidation [12]; and biological methods mainly include the activated sludge method [13]. Previous studies have shown that trace amounts of PEDCs in the actual water environment cannot be effectively removed by conventional water treatment methods and produce by-products with higher endocrine disrupting effects, requiring the use of highly efficient adsorbent materials for the removal and recovery of PEDCs from the aqueous environment with high recognition, selectivity, and rapid adsorption kinetics for PEDCs [14–16]. Therefore, the establishment of efficient methods for the removal of phenolic endocrine disruptors from the aqueous environment is essential to assess their environmental persistence and estrogenic activity.

Molecularly imprinted polymers (MIPs) are supramolecular materials with specific recognition that have been widely used in some research fields, such as separation [17], catalysis [18], analytical chemistry [19], and biosensing [20]. Molecularly imprinted polymers are formed by co-polymerizing template molecules and functional monomers using cross-linking agents and then cleaning the template molecules by organic solvent extraction. This imprinting process creates “imprinted pores” that match the size, shape and physicochemical properties of the template molecule and are capable of repeatedly binding and recognizing the molecule in the presence of other interfering molecules [21,22]. Thus, MIPs are characterized by high affinity and selective binding to target molecules, similar to natural receptors. The super cross-linked rigid structure that MIPs have enables them to be stable in physical and chemical environments with high temperatures, high pressure, acidic or alkaline surroundings, and organic solvents [23,24].

In recent years, molecular imprinting technology has been widely used in the field of water environment treatment, using the selectivity of MIPs to identify and remove PEDCs from the water environment [25–28]. Usually, most of the MIPs synthesized by traditional free radical polymerization techniques are blocky and granular three-dimensional structures with a wide size distribution, and the template molecules encapsulated inside the MIPs may be left behind during the elution and extraction process [29,30]. Although such MIPs have high affinity and selectivity, their adsorption capacity and precision for target molecule adsorption sites need to be improved. In order to achieve the rapid “capture” of PEDCs by MIPs, MIPs are prepared into two-dimensional film structures by surface molecular imprinting [31–35], which can avoid the “leakage” of template molecules that may occur during the adsorption process of conventional three-dimensional MIPs [36–38], and improving the selectivity and sensitivity of MIPs films to target molecules, thus enabling fast and accurate selective identification of PEDCs in adsorbed aqueous environments [39–41].

Graphene has received widespread attention for its unique two-dimensional nanostructure and holds great promise for application in the field of nanoscience and technology [42]. Due to the limitations of existing physical methods, chemical modifications are usually used to further improve the physicochemical properties of graphene [43]. Research on functionalized graphene composites synthesized by selecting graphene materials as a matrix and combining them with nanoparticles, polymer materials, and magnetic materials is developing rapidly [44]. The composites combine many properties of graphene materials and functional molecules, demonstrate good biocompatibility, and are widely used in research fields such as electrochemistry, biology, and materials science [45]. Among them, magnetic graphene-based materials have proven to be a simple, convenient and effective method for the separation and purification of biological samples and the removal of organic contaminants from the aqueous environment because of the unique magnetic properties of magnetic materials and their ability to be separated from samples under the action of an applied magnetic field [46]. In our previous research work, we explored the interactions between graphene, functional monomers, and template molecules using density flooding theory simulations and found that the introduction of graphene provides a significant  $\pi$  surface that can overlap with the  $\pi$  orbitals of template molecules and the resulting

$\pi$ - $\pi$  conjugation effect can enhance the stability of the functional monomers and template molecules bound to each other [47].

On the other hand, metal-organic frameworks (MOFs) are emerging porous materials that have been explored as efficient adsorbents due to their ultra-high surface area, high porosity, tunable pore structure, and chemical modification capabilities and have become a research hotspot in many fields [48–51]. Among them, zeolitic imidazolate frameworks are a class of MOFs with zeolite topology formed by ligating nitrogen-containing heterocyclic imidazoles and their derivatives with metal ions. Chaitali et al. reported that a highly sensitive and selective doubly imprinted polymer-modified electrochemical sensor based on a copper metal-organic framework/mesoporous carbon (Cu-MOF/MC) composite was developed for the simultaneous determination of rifampicin (RIF) and isoniazid (INZ) [52]. Compared with MOFs, ZIFs have higher thermal stability and adsorption capacity, and the composites combining them with functional materials such as graphene and magnetic nanoparticles have higher adsorption capacity and magnetic separation performance [53–56]. Among them, ZIF-8 and ZIF-7, which are ligand-bound to imidazole-like anions via  $\text{Zn}^{2+}$ , are typical framework structures among many ZIFs materials. Yang et al. successfully prepared molecularly imprinted hybrid materials with good selective recognition of 2,4-dichlorophenoxyacetic acid (2,4-D) by combining ZIF-8 with MIPs by emulsion polymerization [57]. In contrast, the sodalite topology and hexagonal spatial structure of ZIF-7 provide it with good chemical stability in organic solvents, water, and alkaline solutions [58], and it is widely used in the research fields of hydrogen storage, adsorption, separation, and catalysis due to its simple preparation method and controllable nanocrystal size and phase appearance [59,60].

Based on the above considerations, this study used ZIFs and  $\text{Fe}_3\text{O}_4$ -modified graphene to obtain magnetic graphene composites with high adsorption capacity and combined surface molecular imprinting technology with magnetic graphene composites to obtain highly efficient heterogeneous adsorption materials. MRGO@ZIF-MIP, due to the combination of the properties of magnetic graphene, ZIFs, and MIPs, provides an effective strategy for highly selective, high adsorption efficiency for the removal of PEDCs in the aqueous environment and has great application prospects in the treatment and prevention of pollution in the aqueous environment.

## 2. Experiment Section

### 2.1. Materials

Ferric chloride hexahydrate ( $\text{FeCl}_3 \cdot 6\text{H}_2\text{O}$ ), sodium acetate (NaOAc), and graphite were obtained from Sigma-Aldrich (Shanghai, China). BPA,  $17\beta$ -estradiol ( $17\beta\text{-E}_2$ ), progesterone (P4), and phenol were purchased from Alfa Aesar (Beijing, China). Acrylamide (Aam), azobisisobutyronitrile (AIBN), divinylbenzene (DVB), and the other chemicals used in the experiments were all from Tianjin Chemical Reagent Co (Tianjin, China). For the actual water samples, tap water was taken from the water supply system, lake water was taken from the artificial lake on our campus, and Haihe water was taken from the Haihe River in Tianjin.

### 2.2. Synthesis of GO and MRGO

Graphene oxide (GO) was prepared from graphite according to the modified Hummers method [47]. Firstly, the reaction was carried out by mixing 3 g of graphite powder, 1.5 g of  $\text{NaNO}_3$ , and 69 mL of concentrated  $\text{H}_2\text{SO}_4$ , adding 9 g of  $\text{KMnO}_4$  and reacting at  $10^\circ\text{C}$  for 2 h. Secondly, 138 mL of distilled water was slowly added dropwise to the three-neck flask with a constant pressure dropping funnel, followed by the reaction for 1 h. Finally, the reaction was terminated by slowly adding an appropriate amount of  $\text{H}_2\text{O}_2$  and secondary water, and the product was repeatedly washed to neutral and freeze-dried.

$\text{Fe}_3\text{O}_4$ /reduced GO (MRGO) was obtained according to a previously reported method with slight modifications [61,62]. Firstly, 1.62 g of  $\text{FeCl}_3 \cdot 6\text{H}_2\text{O}$  was dissolved in 40 mL of a mixture of ethylene glycol and diethylene glycol and sonicated for 10 min. Secondly,

100 mg GO, 0.3529 g sodium citrate, and 4.32 g anhydrous sodium acetate were added to the above mixture and continued to be sonicated for 30 min. Finally, the reaction was loaded into a polytetrafluoroethylene reactor and carried out at 200 °C. The products were washed three times each with distilled water and anhydrous ethanol and dried under a vacuum.

### 2.3. Synthesis of MRGO@ZIF-7

We prepared 0.487 g  $\text{Zn}(\text{NO}_3)_2 \cdot 6\text{H}_2\text{O}$  dissolved in 15 mL DMF and 0.515 g benzimidazole dissolved in 15 mL DMF; ultrasonication was carried out for 10 min. The mixed solution containing MRGO was placed in an oil bath at 120 °C for 2.5 h to crystallize. After cooling to room temperature, the resultant product was isolated by an external magnetic field and washed with methanol and ethanol. Finally, the MRGO@ZIF-7 was dried in a vacuum oven.

### 2.4. Synthesis of MRGO@ZIF7-MIP, MRGO@ZIF7-NIP, and MRGO-MIP

We dissolved 0.1 g of MRGO@ZIF-7 and MRGO in approximately 100 mL of toluene, and it was dispersed ultrasonically for 30 min. Subsequently, bisphenol A, acrylamide, and divinylbenzene 11.36 mL were ultrasonicated for 20 min, and we added a small amount of azo diisobutyronitrile to the reaction system. Oxygen was removed from the reaction system by nitrogen, and the reaction was carried out at 60 °C for 24 h. The products were washed several times with toluene and acetic acid/methanol (1/9, *v/v*) solutions, respectively, until no BPA was detected. The products MRGO@ZIF7-MIP and MRGO-MIP were obtained after vacuum drying at 60 °C for 24 h. The non-imprinted polymer (MRGO@ZIF7-NIP) was prepared in the same way as the imprinted polymer, except that the template molecule bisphenol A was not added to the reaction system.

### 2.5. Characterization

The morphology of the products was characterized by transmission electron microscopy (TEM, TECNIG20, 200 kV, USA) and scanning electron microscopy (SEM, S4800HSD, Japan). X-ray diffraction (XRD) analysis was recorded on an XRD-6100 (Japan). Brunner–Emmet–Teller (BET) spectra were recorded on a V-Sorb X800 (China) Raman spectrometer (Jobin Yvon HR 800, French). Magnetic properties were measured with a LakeShore 7307 (Lakeshore Cryotronic, USA) vibration sample magnetometer (VSM) at 300 K.

### 2.6. Adsorption Measurement

In the next step, 20 mg MRGO@ZIF7-MIP, MRGO-MIP, and MRGO@ZIF7-NIP were dispersed to 0.08 mmol L<sup>-1</sup> BPA (20 mL) in aqueous solution, and the kinetic processes of BPA adsorption by these three materials were investigated. The experimental procedure was performed under continuous shaking at 25 °C, and samples were collected for testing at different time intervals of 5, 10, 20, 30, 40, 50, 80, and 60 min. The adsorption amounts of MRGO@ZIF7-MIP, MRGO-MIP, and MRGO@ZIF7-NIP were calculated based on the difference in concentration before and after the adsorption of BPA. In order to investigate the equilibrium process of the adsorption of MRGO@ZIF7-MIP, MRGO-MIP, and MRGO@ZIF7-NIP on template molecules, 10 mg of the three materials were adsorbed into different initial concentrations (0.01–0.2 mmol L<sup>-1</sup>) of BPA solution for 1 h, and the sample concentrations were detected at 279 nm with a UV-Vis spectrophotometer (Helios-β). To evaluate the selectivity of experimental materials for BPA [35], 10 mg MRGO@ZIF7-MIP and MRGO@ZIF7-NIP were dispersed in 10 mL of mixed aqueous solution containing 0.08 mmol L<sup>-1</sup> of BPA, 17β-E<sub>2</sub>, phenol, and progesterone (P4). The concentrations of BPA, 17β-E<sub>2</sub>, progesterone (P4), and phenol in the samples were measured by a UV-Vis spectrophotometer after 1 h of adsorption equilibration. In addition, 10 mg MRGO@ZIF7-MIP and MRGO@ZIF7-NIP were dispersed in running water, lake water, or Haihe river solution of 0.08 mmol L<sup>-1</sup> BPA (10 mL). After 1 h, The concentration of the BPA was measured by a UV-Vis spectrophotometer. At the same time, we analyzed the different pH values,

temperatures and catalysts on the material, taking note of their influence on adsorption performance. The amounts of the adsorbed BPA were calculated and expressed as  $Q$  (mg/g) according to Equation (1).

$$Q = (C_0 - C_e)V/W \quad (1)$$

where  $C_0$  and  $C_e$  (mg/mL) are the initial and equilibrium concentrations of the BPA, respectively,  $V$  (mL) is the volume of the BPA sample solution, and  $W$  (g) is the mass of adsorbent material used [63].

### 3. Results and Discussion

#### 3.1. Structure and Morphology

The morphology and structure are explored by SEM and TEM for MRGO, MRGO@ZIF-7, and MRGO@ZIF7-MIP, as shown in Figure 1. Figure 1a shows the SEM and TEM (inset) images of sample MRGO.  $\text{Fe}_3\text{O}_4$  microspheres are uniformly distributed on the RGO surface with an average particle size of about 200 nm. Figure 1b shows the SEM and TEM (inset) images of sample MRGO@ZIF-7, where  $\text{Fe}_3\text{O}_4$  and ZIF-7 have adhered well to the surface of wrinkled RGO. ZIF-7 demonstrates a three-dimensional block structure, smooth surface, and an average particle size of around 400 nm. Figure 1c shows SEM and TEM (inset) images of sample MRGO@ZIF7-MIP; the description shows that ZIF-7 and MRGO are covered by molecularly imprinted polymers when MIP is grafted onto the MRGO@ZIF-7 surface.

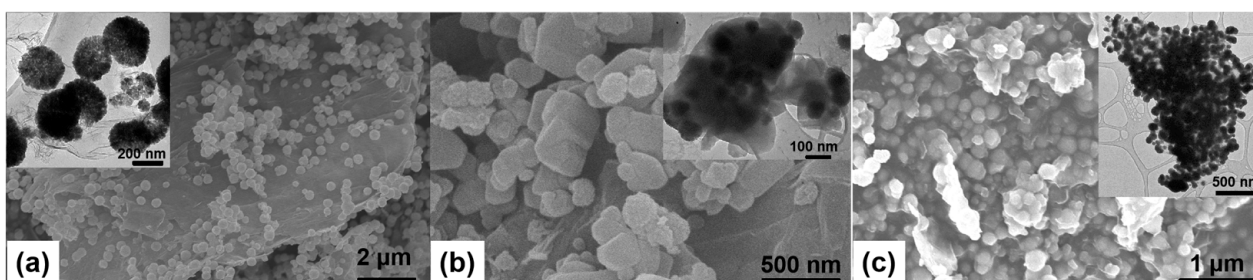


**Figure 1.** Morphology of (a) MRGO, (b) MRGO@ZIF-7, and (c) MRGO@ZIF7-MIP.

The structural properties of the prepared experimental materials were characterized using the XRD technique (Figure 2). For MRGO, the peaks represent the Bragg reflections of (220), (311) and (400) facets, which match well with those of  $\text{Fe}_3\text{O}_4$  nanoparticles (JCPDS Card No. 19-0629), indicating the coating of  $\text{Fe}_3\text{O}_4$  microspheres on RGO [61]. After the decoration of ZIF-7, typical diffraction peaks of ZIF-7 emerge, consistent with the reference XRD pattern for the cubic ZIF-7 (CCDC Card No. 04-2541) [54]. Furthermore, the crystal plane diffraction peaks of  $\text{Fe}_3\text{O}_4$  microspheres can also be observed. These observations suggest that the introduction of ZIF-7 did not affect the crystalline structure of MRGO. When MIP was grafted onto the surface of MRGO@ZIF-7, the positions and widths of the diffraction peaks did not change, indicating that the crystalline structures of the  $\text{Fe}_3\text{O}_4$  microspheres and ZIF-7 were not affected by the grafted MIP.

Analytical characterization was carried out regarding the specific surface area, total pore volume, and pore size distribution of experimental materials using the BET adsorption equation and BJH academic model. The nitrogen adsorption-desorption isotherms and pore size distributions of MRGO@ZIF7-MIP, MRGO@ZIF-7, and MRGO were analyzed, as shown in Figure 3. Figure 3a shows that the Brunauer–Emmett–Teller (BET) surface areas of MRGO@ZIF-7, MRGO@ZIF7-MIP, and MRGO are  $261.31 \text{ m}^2 \text{ g}^{-1}$ ,  $96.83 \text{ m}^2 \text{ g}^{-1}$ , and  $51.98 \text{ m}^2 \text{ g}^{-1}$ , respectively. The introduction of ZIF-7 in the MRGO@ZIF-7 structure resulted in a significant increase in the specific surface area compared to MRGO [55], and the decrease in the specific surface area when its surface was grafted with MIP again proved the presence of MIP. In addition, all three materials exhibit type-IV adsorption isotherms, and their mesoporous structures are an important basis for their efficient ad-

sorption performance. Figure 3b,c shows the pore size distribution of MRGO@ZIF-7 and MRGO@ZIF7-MIP. Both materials have a uniformly distributed pore structure with an average pore size of 1.848 nm and 3.823 nm, respectively.

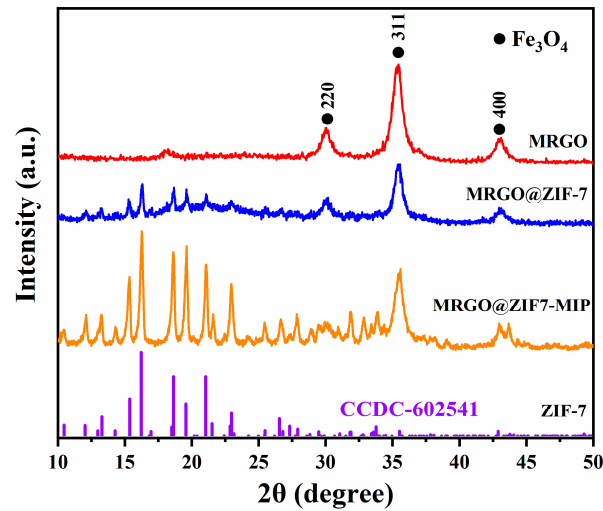


**Figure 2.** XRD patterns of MRGO, MRGO@ZIF-7 and MRGO@ZIF7-MIP.

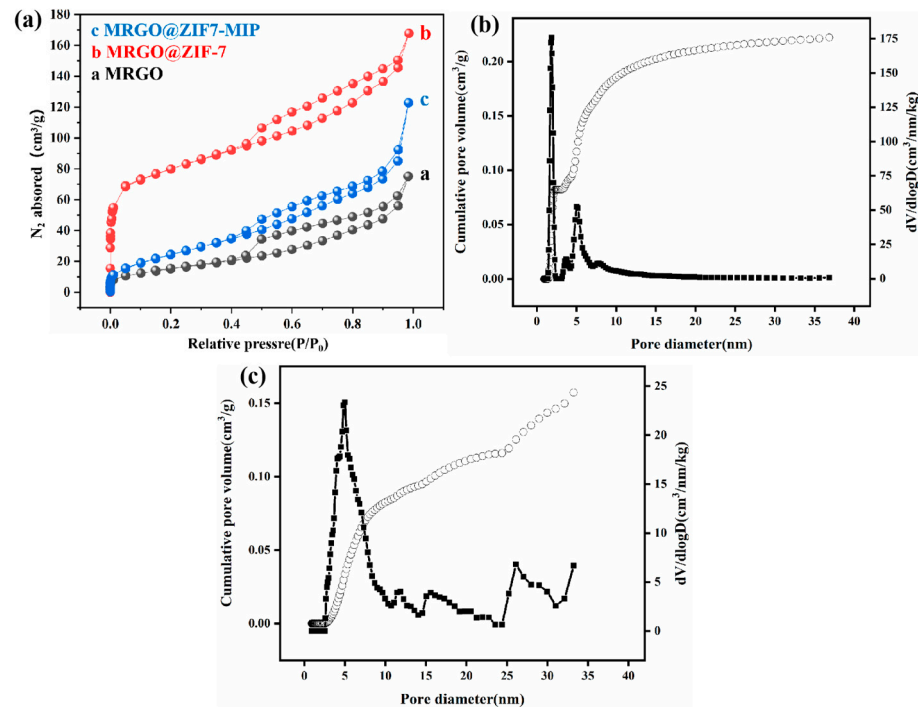


**Figure 3.** (a) The nitrogen adsorption–desorption isotherms of MRGO@ZIF7-MIP, MRGO@ZIF-7 and MRGO and (b,c) pore size distribution of MRGO@ZIF-7 and MRGO@ZIF7-MIP.

Raman spectroscopy is an effective method for characterizing the structure and properties of graphene materials, such as surface defects, edge structures, and doping states. Figure 4a shows the Raman spectra of MRGO, MRGO@ZIF-7, and MRGO@ZIF7-MIP. Two distinct absorption peaks appear in the spectra of all three materials for the G and D peaks, respectively. The G peak is the main characteristic peak of graphene materials, which is caused by the in-plane vibration of  $sp^2$  carbon atoms and appears near  $1580\text{ cm}^{-1}$  [64]. The D peak is usually considered the disordered vibrational peak of graphene materials, which is caused by the lattice vibrations leaving the center of the Brillouin zone. It is used to characterize the structural defects on the surface of graphene materials and appears near

1370  $\text{cm}^{-1}$  [65]. Compared with MRGO and MRGO@ZIF-7, the D-band of RGO@ZIF7-MIP was the widest, indicating that the disorder of graphene layers gradually increased during the functionalization modification. By comparing the G-bands of the three materials, it can be seen that the G-peaks of both RGO@ZIF7-MIP and MRGO@ZIF-7 are blue-shifted compared to those of MRGO, indicating that there is an interaction between ZIF-7, MIP, and magnetic graphene, which provides evidence for the successful preparation of the various materials. In addition, the intensity ratio ( $I_D/I_G$ ) is characteristic of the extent of disorder present within the material [66]. The calculated  $I_D/I_G$  ratios for the three materials are 1.04, 1.07 and 1.1, respectively, which again indicate the increase in surface disorder of graphene materials. Figure 4b shows the magnetic hysteresis loop of MRGO, MRGO@ZIF-7, and RGO@ZIF7-MIP. All three materials have good magnetic properties, and the saturation magnetization intensity of MRGO is the largest ( $74.97 \text{ emu g}^{-1}$ ). The magnetic intensity of the composites gradually decreases after the gradual modification of ZIF-7 and MIP on their surfaces. The saturation magnetization intensity of RGO@ZIF7-MIP is minimal ( $4.84 \text{ emu g}^{-1}$ ) and still has the magnetic properties required for magnetic separation. Effective magnetic separation can be observed after about 80 s under the action of an external magnetic field, as shown in Figure 4b (bottom inset).

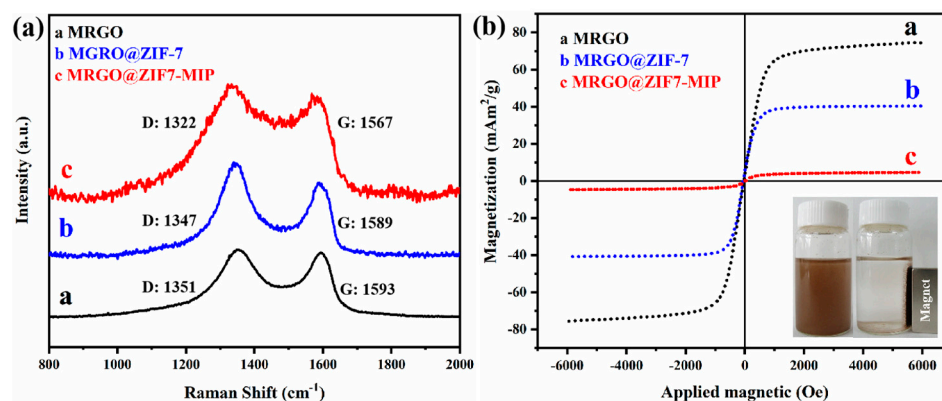


**Figure 4.** (a) Raman spectra and (b) magnetic hysteresis loop of the MRGO, MRGO@ZIF-7, and RGO@ZIF7-MIP. The inset shows the separation process of the RGO@ZIF7-MIP solution under the action of an external magnetic field.

### 3.2. Adsorption of BPA onto MRGO@ZIF7-MIP

#### 3.2.1. Factors Affecting Adsorption

Adsorbent dosage is an important factor in deciding the adsorption time. In this work, the adsorbent dosage was evaluated in the range of 1–20 mg, and the results are shown in Figure 5a. It can be seen that the adsorption capacity was increased as the adsorbent dosage gradually increased. When the amount of adsorbent is 10 mg, the saturation point of adsorption is almost reached, and the adsorption amount of MRGO@ZIF7-NIP is less than MRGO@ZIF7-MIP. In the experiment, the MRGO@ZIF7-NIP and MRGO@ZIF7-MIP were set as a control group to optimize the temperature of the adsorbent for the adsorption process. As shown in Figure 5b, when the temperature increased to 25 °C, the adsorption capacity of MRGO@ZIF7-MIP composites is the largest. Although the adsorption capacity of MRGO@ZIF7-NIP increased as the temperature gradually increased, the increment was not obvious, and it may be due to the fact that the higher the temperature in the adsorption experiment, the higher the kinetic energy of the molecules and the more violent the irregular motion of the molecules [18]. Therefore, we carried out adsorption experiments at 25 °C. Figure 5c shows the effect of pH on the adsorption of BPA. The pH of the solution plays an important role in affecting the adsorption characteristics of BPA. When the solution pH value is about 7, that is close to neutral when the adsorption capacity of the adsorbent is the strongest. The adsorption capacity is less when the solution gradually becomes alkaline. It may be due to the weak acidity of BPA, which is easily neutralized when the solution

becomes more basic. In a word, the adsorbent adsorption environment should try to control the neutral.

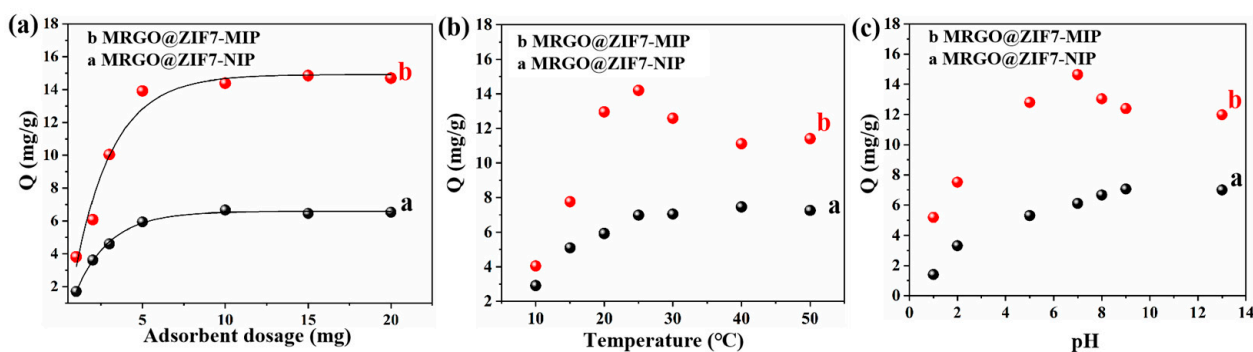


**Figure 5.** Adsorption effect of different factors: adsorbent dosage (a), temperature (b), pH (c). Other conditions: 10 mL sample solution of  $0.08 \text{ mmol L}^{-1}$  BPA.

### 3.2.2. Adsorption Kinetics

To investigate the binding properties of molecularly imprinted materials to template molecules, we performed an adsorption kinetic analysis of BPA using MRGO@ZIF7-MIP, MRGO-MIP, and MRGO@ZIF7-NIP, and the results are shown in Figure 6. It can be clearly seen that the adsorption process of the three materials on BPA was divided into two stages, the adsorption efficiency was faster from 0 to 15 min, the adsorption amount increased significantly with time, and the adsorption rate slowed down significantly after 15 min and gradually reached the adsorption equilibrium. In contrast, MRGO@ZIF7-MIP showed the best adsorption performance, and the specific recognition sites present on the surface of both MRGO@ZIF7-MIP and MRGO-MIP facilitated the adsorption recognition of BPA, and the adsorption capacity was superior to that of MRGO@ZIF7-NIP.

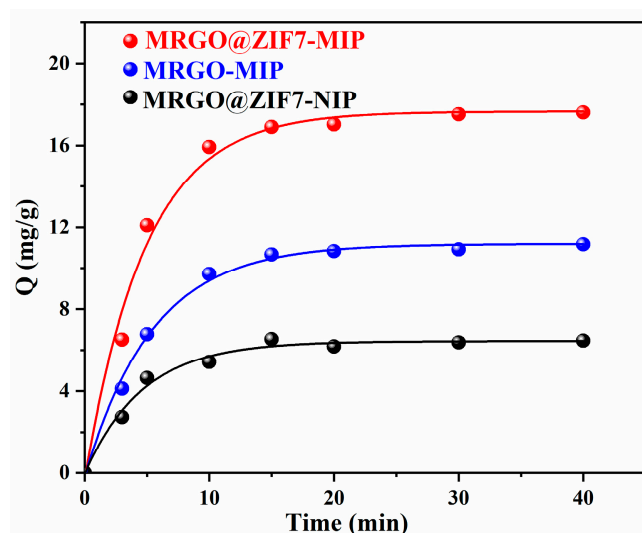


**Figure 6.** Adsorption kinetic curve of MRGO@ZIF7-MIP, MRGO-MIP, and MRGO@ZIF7-NIP for BPA. Other conditions: 20 mg sorbent, 20 mL sample solution of  $0.08 \text{ mmol L}^{-1}$  BPA, temperature  $25 \text{ }^\circ\text{C}$ .

### 3.2.3. Sorption Isotherm

The adsorption capacity is an important parameter that reflects the performance of the adsorbent and determines the amount of adsorbent required during the adsorption experiment. The adsorption capacity of the adsorbent on the template molecules can be analyzed by the adsorption isotherm. The adsorption isotherms of BPA by MRGO@ZIF7-MIP, MRGO-MIP and MRGO@ZIF7-NIP are presented in Figure 7. The Langmuir isotherm

model was adopted to fit the experimental data. The  $Q_e$  are correlated with the isotherm model of Langmuir to Equation (2):

$$1/Q_e = 1/Q_{\max} + C_e/bQ_{\max} \quad (2)$$

where  $Q_e$  (mg/g) is the adsorbed amount of BPA,  $Q_{\max}$  (mg/g) is the maximum adsorbing capacity,  $b$  is the adsorption equilibrium constant, and  $C_e$  (mg/mL) is the equilibrium concentration [67].

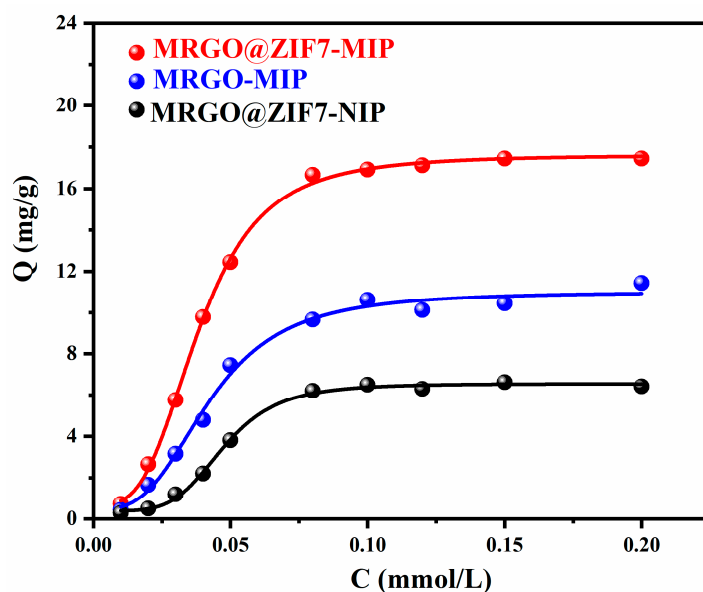


**Figure 7.** Adsorption isotherms of MRGO@ZIF7-MIP, MRGO-MIP, and MRGO@ZIF7-NIP for BPA. Other conditions: 10 mg sorbent, 10 mL sample solution of  $0.08 \text{ mmol L}^{-1}$  BPA, temperature  $25 \text{ }^\circ\text{C}$ .

As shown in Figure 7, the adsorption of BPA by MRGO@ZIF7-MIP and MRGO-MIP were both better than that by MRGO@ZIF7-NIP and increased significantly with the increase in the initial concentration of BPA. Calculated with the isotherm model of Langmuir, the maximum adsorption amount of MRGO@ZIF7-MIP, MRGO-MIP, and MRGO@ZIF7-NIP for BPA was 24.32, 15.46 and 6.34 mg/g, respectively. MRGO@ZIF7-MIP showed the highest adsorption amount, about 1.6 times that of MRGO-MIP and about 4 times that of MRGO@ZIF7-NIP. The results of adsorption isotherm analysis again indicate that the adsorption sites present on the surface of molecularly imprinted polymers have good molecular recognition of BPA.

#### 3.2.4. Competitive Adsorption, Reuse, and Analysis of Environmental Water Samples

$17\beta\text{-E}_2$ , phenol and progesterone (P4), which are structurally similar to BPA, were selected as interferences to evaluate the selective recognition of BPA by MRGO@ZIF7-MIP. As shown in Figure 8, the removal efficiency of BPA,  $17\beta\text{-E}_2$ , phenol, and progesterone (P4) can reach 85.92%, 35.14%, 29.82%, and 19.10%, respectively, after being treated with MRGO@ZIF7-MIP. The molecularly imprinted polymer structure has “imprinting pores” that match the size and shape of the template molecule. The active site in the “imprinted pore” is able to bind specifically to the target molecule, resulting in MRGO@ZIF7-MIP exhibiting excellent selectivity for BPA. However, the MRGO@ZIF7-NIP has no selectivity; its effect on the removal efficiency of BPA,  $17\beta\text{-E}_2$ , phenol and progesterone (P4) is similar (25.14%, 19.04%, 16.14%, 10.32%, respectively). The results of the selectivity study indicate that molecularly imprinted nanofilms do have highly sensitive recognition of template molecules.

In addition, we performed 5 cycles of adsorption experiments on BPA using MRGO@ZIF7-MIP to evaluate its stability and reusability. The adsorption results of repeated uses in

MRGO@ZIF7-MIP are shown in Figure 9. The MRGO@ZIF7-MIP can be reused after extraction with an acetic acid/methanol (1/9, *v/v*) mixture, and no obvious decrease in the adsorption capacity was observed. The adsorption capacity of MRGO@ZIF7-MIP for BPA slightly decreased during 5 cycles of adsorption, which might be related to the loss of memory cavity during regeneration. The study showed that MRGO@ZIF7-MIP has good stability and can be reused.

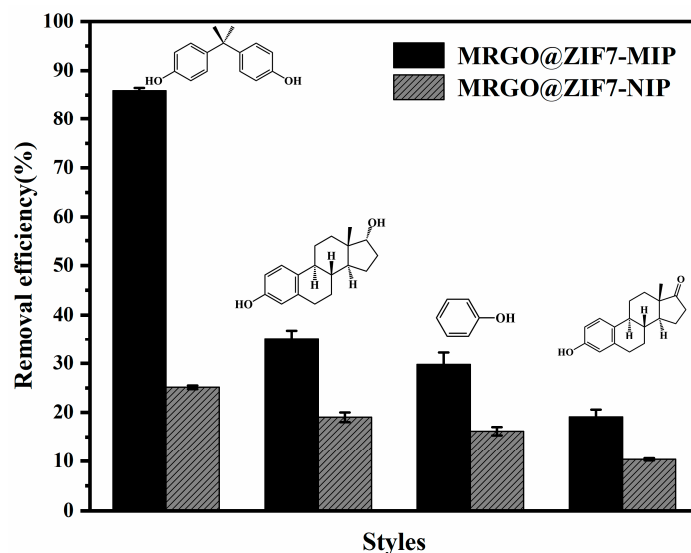


**Figure 8.** Removal efficiency of interfering molecules. Other conditions: 10 mg sorbent, 10 mL sample solution, shaking time 1 h, temperature 25 °C.

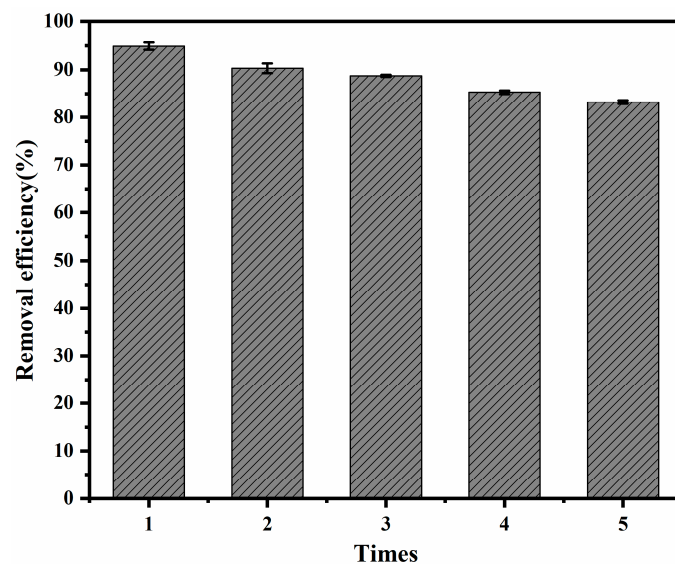


**Figure 9.** Stability and repeatability of the MRGO@ZIF7-MIP. Other conditions: 10 mg sorbent, 10 mL sample solution of 0.08 mmol L<sup>-1</sup> BPA, temperature 25 °C.

Tap water, lake water and sea river containing 0.08 mmol L<sup>-1</sup> BPA were selected as “simulated” wastewater to investigate the adsorption selection performance of MRGO@ZIF7-MIP in the real water environment. As seen in Figure 10, the MRGO@ZIF7-MIP can produce good recovery, and the removal efficiencies of BPA are 72.07%, 57.84% and 51.26%, respectively. The results show that the imprinted polymer present on the surface of MRGO@ZIF7-MIP has good specific molecular recognition ability for BPA and can be effectively applied to remove phenolic endocrine disruptors from the actual aqueous environment.

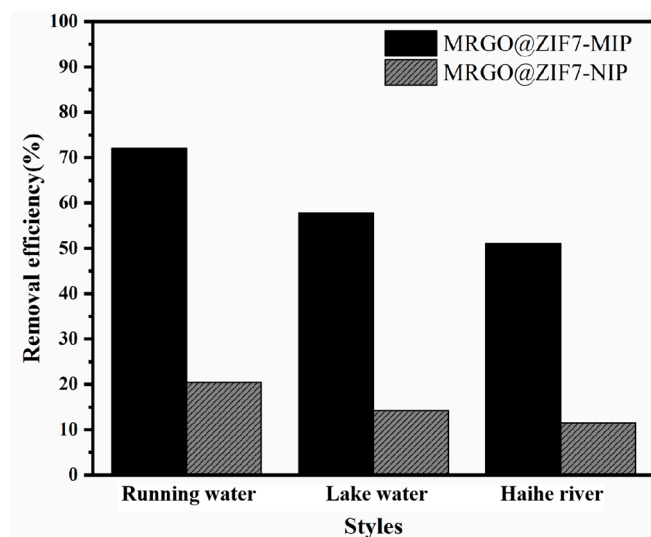


**Figure 10.** Adsorption of MRGO@ZIF7-MIP for BPA in “simulated” wastewater. Other conditions: 10 mg sorbent, 10 mL “simulated” wastewater of 0.08 mmol L<sup>-1</sup> BPA, temperature 25 °C.

#### 4. Conclusions

In this paper, we provide a surface molecular imprinting method to produce an MRGO@ZIF-7-based detecting platform. The as-synthesized MRGO@ZIF7-MIP showed obvious molecular imprinting effects towards the template, fast template rebinding kinetics, and an appreciable selectivity over the interferents. Although the results reported here relate only to BPA, the principles of the as-proposed methodology are expected to be applicable to the removal of other PEDCs from contaminated water. We believe that the potential of the molecular imprinting technique for the fast and selective removal of phenolic endocrine-disrupting chemicals from aqueous environments.

**Author Contributions:** Methodology, Y.L. (Yang Li), Z.D. and Z.G.; validation, Y.L. (Ying Li), D.W. and Y.S.; formal analysis, Y.L. (Yang Li); investigation, D.W.; data curation, Y.L. (Ying Li), Y.L. (Yang Li), Z.D. and Z.G.; writing—original draft preparation, Y.L. (Ying Li), Y.L. (Yang Li), Z.D. and Y.L. (Ying Liu); writing—review and editing, Y.L. (Ying Li) and Y.L. (Ying Liu); supervision, D.W. All authors have read and agreed to the published version of the manuscript.

**Funding:** This research received no external funding.

**Data Availability Statement:** Not applicable.

**Acknowledgments:** This work was supported by the National Natural Science Foundation of China (22078246, 22178270).

**Conflicts of Interest:** The authors declare no conflict of interest.

#### References

1. Metcalfe, C.D.; Bayen, S.; Desrosiers, M.; Munoz, G.; Sauve, S.; Yargeau, V. An introduction to the sources, fate, occurrence and effects of endocrine disrupting chemicals released into the environment. *Environ. Res.* **2022**, *207*, 112658. [[CrossRef](#)]
2. Wang, R.; Ma, X.; Liu, T.; Li, Y.; Song, L.; Tjong, S.C.; Cao, L.; Wang, W.; Yu, Q.; Wang, Z. Degradation aspects of endocrine disrupting chemicals: A review on photocatalytic processes and photocatalysts. *Appl. Catal. A Gen.* **2020**, *597*, 117547. [[CrossRef](#)]
3. Deng, Z.-H.; Li, N.; Jiang, H.-L.; Lin, J.-M.; Zhao, R.-S. Pretreatment techniques and analytical methods for phenolic endocrine disrupting chemicals in food and environmental samples. *TrAC Trends Anal. Chem.* **2019**, *119*, 115592. [[CrossRef](#)]
4. Chen, Y.; Xie, H.; Junaid, M.; Xu, N.; Zhu, Y.; Tao, H.; Wong, M. Spatiotemporal distribution, source apportionment and risk assessment of typical hormones and phenolic endocrine disrupting chemicals in environmental and biological samples from the mariculture areas in the Pearl River Delta, China. *Sci. Total Environ.* **2022**, *807*, 150752. [[CrossRef](#)] [[PubMed](#)]
5. Jing, X.; He, J.; Zhao, W.; Huang, X.; Wang, X. Effervescent tablet-assisted switchable hydrophilicity solvent-based microextraction with solidification of floating organic droplets for HPLC determination of phenolic endocrine disrupting chemicals in bottled beverages. *Microchem. J.* **2020**, *155*, 104680. [[CrossRef](#)]

6. Barich, H.; Cánovas, R.; De Wael, K. Electrochemical identification of hazardous phenols and their complex mixtures in real samples using unmodified screen-printed electrodes. *J. Electroanal. Chem.* **2022**, *904*, 115878. [[CrossRef](#)]
7. Adegoke, K.A.; Olagunju, A.O.; Alagbada, T.C.; Alao, O.C.; Adesina, M.O.; Afolabi, I.C.; Adegoke, R.O.; Bello, O.S. Adsorptive Removal of Endocrine-Disrupting Chemicals from Aqueous Solutions: A Review. *Water Air Soil Pollut.* **2022**, *233*, 38. [[CrossRef](#)]
8. Li, Q.; Chai, C.; Zhao, L. Biodegradation of Endocrine Disrupting Chemicals with Laccase Isozymes from Recombinant *Pichia pastoris*. *Catal. Lett.* **2021**, *152*, 2625–2636. [[CrossRef](#)]
9. Vrachnis, N.; Loukas, N.; Vrachnis, D.; Antonakopoulos, N.; Zygouris, D.; Komicronlialexi, A.; Pergalotis, V.; Iavazzo, C.; Mastorakos, G.; Iliodromiti, Z. A Systematic Review of Bisphenol A from Dietary and Non-Dietary Sources during Pregnancy and Its Possible Connection with Fetal Growth Restriction: Investigating Its Potential Effects and the Window of Fetal Vulnerability. *Nutrients* **2021**, *13*, 2426. [[CrossRef](#)]
10. Lv, Y.Z.; Yao, L.; Wang, L.; Liu, W.R.; Zhao, J.L.; He, L.Y.; Ying, G.G. Bioaccumulation, metabolism, and risk assessment of phenolic endocrine disrupting chemicals in specific tissues of wild fish. *Chemosphere* **2019**, *226*, 607–615. [[CrossRef](#)]
11. Xiang, W.; Qu, R.; Wang, X.; Wang, Z.; Bin-Jumah, M.; Allam, A.A.; Zhu, F.; Huo, Z. Removal of 4-chlorophenol, bisphenol A and nonylphenol mixtures by aqueous chlorination and formation of coupling products. *Chem. Eng. J.* **2020**, *402*, 126140. [[CrossRef](#)]
12. Cantarella, M.; Carroccio, S.C.; Dattilo, S.; Avolio, R.; Castaldo, R.; Puglisi, C.; Privitera, V. Molecularly imprinted polymer for selective adsorption of diclofenac from contaminated water. *Chem. Eng. J.* **2019**, *367*, 180–188. [[CrossRef](#)]
13. Zhang, Y.; Lei, Y.; Lu, H.; Shi, L.; Wang, P.; Ali, Z.; Li, J. Electrochemical detection of bisphenols in food: A review. *Food Chem.* **2021**, *346*, 128895. [[CrossRef](#)] [[PubMed](#)]
14. Wang, X.; Xiang, W.; Wang, S.; Ge, J.; Qu, R.; Wang, Z. Oxidative Oligomerization of Phenolic Endocrine Disrupting Chemicals Mediated by Mn(III)-L Complexes and the Role of Phenoxy Radicals in the Enhanced Removal: Experimental and Theoretical Studies. *Environ. Sci. Technol.* **2020**, *54*, 1573–1582. [[CrossRef](#)] [[PubMed](#)]
15. Palacios Colon, L.; Rascon, A.J.; Hejji, L.; Azzouz, A.; Ballesteros, E. Validation and Use of an Accurate, Sensitive Method for Sample Preparation and Gas Chromatography-Mass Spectrometry Determination of Different Endocrine-Disrupting Chemicals in Dairy Products. *Foods* **2021**, *10*, 1040. [[CrossRef](#)]
16. Zhao, W.; Jing, X.; Tian, Y.; Feng, C. Magnetic Fe<sub>3</sub>O<sub>4</sub>@porous activated carbon effervescent tablet-assisted deep eutectic solvent-based dispersive liquid-liquid microextraction of phenolic endocrine disrupting chemicals in environmental water. *Microchem. J.* **2020**, *159*, 105416. [[CrossRef](#)]
17. Wang, M.; Liang, S.; Bai, L.; Qiao, F.; Yan, H. Green protocol for the preparation of hydrophilic molecularly imprinted resin in water for the efficient selective extraction and determination of plant hormones from bean sprouts. *Anal. Chim. Acta* **2019**, *1064*, 47–55. [[CrossRef](#)]
18. He, P.; Zhu, H.; Ma, Y.; Liu, N.; Niu, X.; Wei, M.; Pan, J. Rational design and fabrication of surface molecularly imprinted polymers based on multi-boronic acid sites for selective capture glycoproteins. *Chem. Eng. J.* **2019**, *367*, 55–63. [[CrossRef](#)]
19. Neven, L.; Barich, H.; Slegers, N.; Cánovas, R.; Debruyne, G.; De Wael, K. Development of a combi-electrosensor for the detection of phenol by combining photoelectrochemistry and square wave voltammetry. *Anal. Chim. Acta* **2022**, *1206*, 339732. [[CrossRef](#)]
20. Zhang, H.; Tee, J.C.L.; Jaenicke, S.; Gondal, M.A.; Dastageer, M.A.; Basheer, C.; Chuah, G.-K. BiOBrn1-n solid solutions as versatile photooxidation catalysts for phenolics and endocrine disrupting chemicals. *Catal. Today* **2021**, *375*, 547–557. [[CrossRef](#)]
21. Buffon, E.; Stradiotto, N.R. Electrochemical sensor based on molecularly imprinted poly(ortho-phenylenediamine) for determination of hexahydrofarnesol in aviation biokerosene. *Sens. Actuators B Chem.* **2019**, *287*, 371–379. [[CrossRef](#)]
22. Motia, S.; Tudor, I.A.; Ribeiro, P.A.; Raposo, M.; Bouchikhi, B.; El Bari, N. Electrochemical sensor based on molecularly imprinted polymer for sensitive triclosan detection in wastewater and mineral water. *Sci. Total Environ.* **2019**, *664*, 647–658. [[CrossRef](#)] [[PubMed](#)]
23. Motaharian, A.; Hosseini, M.R.M.; Naseri, K. Determination of psychotropic drug chlorpromazine using screen printed carbon electrodes modified with novel MIP-MWCNTs nano-composite prepared by suspension polymerization method. *Sens. Actuators B Chem.* **2019**, *288*, 356–362. [[CrossRef](#)]
24. Zhang, G.; Yu, Y.; Guo, M.; Lin, B.; Zhang, L. A sensitive determination of albumin in urine by molecularly imprinted electrochemical biosensor based on dual-signal strategy. *Sens. Actuators B Chem.* **2019**, *288*, 564–570. [[CrossRef](#)]
25. Bhogal, S.; Mohiuddin, I.; Kaur, K.; Lee, J.; Brown, R.J.C.; Malik, A.K.; Kim, K.H. Dual-template magnetic molecularly imprinted polymer-based sorbent for simultaneous and selective detection of phenolic endocrine disrupting compounds in foodstuffs. *Environ. Pollut.* **2021**, *275*, 116613. [[CrossRef](#)] [[PubMed](#)]
26. Huang, X.-C.; Ma, J.-K.; Wei, S.-L. Preparation and application of a novel magnetic molecularly imprinted polymer for simultaneous and rapid determination of three trace endocrine disrupting chemicals in lake water and milk samples. *Anal. Bioanal. Chem.* **2020**, *412*, 1835–1846. [[CrossRef](#)] [[PubMed](#)]
27. Li, Y.; Li, X.; Li, Y.; Qi, J.; Bian, J.; Yuan, Y. Selective removal of 2,4-dichlorophenol from contaminated water using non-covalent imprinted microspheres. *Environ. Pollut.* **2009**, *157*, 1879–1885. [[CrossRef](#)]
28. Chang, L.; Li, Y.; Chu, J.; Qi, J.; Li, X. Preparation of core-shell molecularly imprinted polymer via the combination of reversible addition-fragmentation chain transfer polymerization and click reaction. *Anal. Chim. Acta* **2010**, *680*, 65–71. [[CrossRef](#)]
29. Zhang, H. Molecularly Imprinted Nanoparticles for Biomedical Applications. *Adv. Mater.* **2020**, *32*, e1806328. [[CrossRef](#)]
30. Arabi, M.; Ostovan, A.; Bagheri, A.R.; Guo, X.; Wang, L.; Li, J.; Wang, X.; Li, B.; Chen, L. Strategies of molecular imprinting-based solid-phase extraction prior to chromatographic analysis. *TrAC Trends Anal. Chem.* **2020**, *128*, 115923. [[CrossRef](#)]

31. Li, F.; Gao, J.; Wu, H.; Li, Y.; He, X.; Chen, L. A Highly Selective and Sensitive Fluorescent Sensor Based on Molecularly Imprinted Polymer-Functionalized Mn-Doped ZnS Quantum Dots for Detection of Roxarsone in Feeds. *Nanomaterials* **2022**, *12*, 2997. [[CrossRef](#)] [[PubMed](#)]
32. Li, F.; Li, X.; Su, J.; Li, Y.; He, X.; Chen, L.; Zhang, Y. A strategy of utilizing Cu(2+)-mediating interaction to prepare magnetic imprinted polymers for the selective detection of celastrol in traditional Chinese medicines. *Talanta* **2021**, *231*, 122339. [[CrossRef](#)] [[PubMed](#)]
33. Zhang, M.; Zhang, X.; He, X.; Chen, L.; Zhang, Y. A self-assembled polydopamine film on the surface of magnetic nanoparticles for specific capture of protein. *Nanoscale* **2012**, *4*, 3141–3147. [[CrossRef](#)] [[PubMed](#)]
34. Wang, X.; Wang, L.; He, X.; Zhang, Y.; Chen, L. A molecularly imprinted polymer-coated nanocomposite of magnetic nanoparticles for estrone recognition. *Talanta* **2009**, *78*, 327–332. [[CrossRef](#)] [[PubMed](#)]
35. Kong, X.; Gao, R.; He, X.; Chen, L.; Zhang, Y. Synthesis and characterization of the core-shell magnetic molecularly imprinted polymers (Fe<sub>3</sub>O<sub>4</sub>@MIPs) adsorbents for effective extraction and determination of sulfonamides in the poultry feed. *J. Chromatogr. A* **2012**, *1245*, 8–16. [[CrossRef](#)]
36. Mehmandoust, M.; Erk, N.; Karaman, C.; Karaman, O. An electrochemical molecularly imprinted sensor based on CuBi<sub>2</sub>O<sub>4</sub>/rGO@MoS<sub>2</sub> nanocomposite and its utilization for highly selective and sensitive for linagliptin assay. *Chemosphere* **2022**, *291*, 132807. [[CrossRef](#)]
37. Ratautaite, V.; Boguzaitė, R.; Brazys, E.; Ramanaviciene, A.; Ciplys, E.; Juozapaitis, M.; Slibinskas, R.; Bechelany, M.; Ramanavicius, A. Molecularly imprinted polypyrrole based sensor for the detection of SARS-CoV-2 spike glycoprotein. *Electrochim. Acta* **2022**, *403*, 139581. [[CrossRef](#)]
38. Li, G.; Qi, X.; Wu, J.; Xu, L.; Wan, X.; Liu, Y.; Chen, Y.; Li, Q. Ultrasensitive, label-free voltammetric determination of norfloxacin based on molecularly imprinted polymers and Au nanoparticle-functionalized black phosphorus nanosheet nanocomposite. *J. Hazard. Mater.* **2022**, *436*, 129107. [[CrossRef](#)]
39. Rebelo, P.; Costa-Rama, E.; Seguro, I.; Pacheco, J.G.; Nouws, H.P.A.; Cordeiro, M.; Delerue-Matos, C. Molecularly imprinted polymer-based electrochemical sensors for environmental analysis. *Biosens. Bioelectron.* **2021**, *172*, 112719. [[CrossRef](#)]
40. Li, Y.; Dong, C.; Chu, J.; Qi, J.; Li, X. Surface molecular imprinting onto fluorescein-coated magnetic nanoparticles via reversible addition fragmentation chain transfer polymerization: A facile three-in-one system for recognition and separation of endocrine disrupting chemicals. *Nanoscale* **2011**, *3*, 280–287. [[CrossRef](#)]
41. Li, Y.; Li, X.; Li, Y.; Dong, C.; Jin, P.; Qi, J. Selective recognition of veterinary drugs residues by artificial antibodies designed using a computational approach. *Biomaterials* **2009**, *30*, 3205–3211. [[CrossRef](#)] [[PubMed](#)]
42. Park, S.; Ruoff, R.S. Chemical methods for the production of graphenes. *Nat. Nanotechnol.* **2009**, *4*, 217–224. [[CrossRef](#)] [[PubMed](#)]
43. Novoselov, K.S.; Geim, A.K.; Morozov, S.V.; Jiang, D.; Zhang, Y.; Dubonos, S.V.; Grigorieva, I.V.; Firsov, A.A. Electric field effect in atomically thin carbon films. *Science* **2004**, *306*, 666–669. [[CrossRef](#)] [[PubMed](#)]
44. Park, S.; An, J.; Piner, R.D.; Jung, I.; Yang, D.; Velamakanni, A.; Nguyen, S.T.; Ruoff, R.S. Aqueous Suspension and Characterization of Chemically Modified Graphene Sheets. *Chem. Mater.* **2008**, *20*, 6592–6594. [[CrossRef](#)]
45. Wakabayashi, K.; Pierre, C.; Dikin, D.A.; Ruoff, R.S.; Ramanathan, T.; Brinson, L.C.; Torkelson, J.M. Polymer–Graphite Nanocomposites: Effective Dispersion and Major Property Enhancement via Solid-State Shear Pulverization. *Macromolecules* **2008**, *41*, 1905–1908. [[CrossRef](#)]
46. Veca, L.M.; Lu, F.; Mezziani, M.J.; Cao, L.; Zhang, P.; Qi, G.; Qu, L.; Shrestha, M.; Sun, Y.P. Polymer functionalization and solubilization of carbon nanosheets. *Chem. Commun.* **2009**, *18*, 2565–2567. [[CrossRef](#)]
47. Li, Y.; Li, X.; Dong, C.; Qi, J.; Han, X. A graphene oxide-based molecularly imprinted polymer platform for detecting endocrine disrupting chemicals. *Carbon* **2010**, *48*, 3427–3433. [[CrossRef](#)]
48. Huang, Y.-F.; Wang, Y.-Q.; Zhao, Q.-S.; Li, Y.; Zhang, J.-M. Facile in situ hydrothermal synthesis of Fe<sub>3</sub>O<sub>4</sub>@MIL-101 composites for removing textile dyes. *RSC Adv.* **2014**, *4*, 47921–47924. [[CrossRef](#)]
49. Huang, Y.-F.; Liu, M.; Wang, Y.-Q.; Li, Y.; Zhang, J.-M.; Huo, S.-H. Hydrothermal synthesis of functionalized magnetic MIL-101 for magnetic enrichment of estrogens in environmental water samples. *RSC Adv.* **2016**, *6*, 15362–15369. [[CrossRef](#)]
50. Huang, Y.-F.; Sun, X.-Y.; Huo, S.-H.; Li, Y.; Zhong, C. Core-shell dual-MOF heterostructures derived magnetic CoFe<sub>2</sub>O<sub>4</sub>/CuO (sub)microcages with superior catalytic performance. *Appl. Surf. Sci.* **2019**, *466*, 637–646. [[CrossRef](#)]
51. Huang, P.; Yao, L.; Chang, Q.; Sha, Y.; Jiang, G.; Zhang, S.; Li, Z. Room-temperature preparation of highly efficient NH<sub>2</sub>-MIL-101(Fe) catalyst: The important role of -NH<sub>2</sub> in accelerating Fe(III)/Fe(II) cycling. *Chemosphere* **2022**, *291*, 133026. [[CrossRef](#)] [[PubMed](#)]
52. Rawool, C.R.; Srivastava, A.K. A dual template imprinted polymer modified electrochemical sensor based on Cu metal organic framework/mesoporous carbon for highly sensitive and selective recognition of rifampicin and isoniazid. *Sens. Actuators B Chem.* **2019**, *288*, 493–506. [[CrossRef](#)]
53. Liu, Y.; Cheng, H.; Cheng, M.; Liu, Z.; Huang, D.; Zhang, G.; Shao, B.; Liang, Q.; Luo, S.; Wu, T.; et al. The application of Zeolitic imidazolate frameworks (ZIFs) and their derivatives based materials for photocatalytic hydrogen evolution and pollutants treatment. *Chem. Eng. J.* **2021**, *417*, 127914. [[CrossRef](#)]
54. Liu, Y.; Huo, Y.; Wang, X.; Yu, S.; Ai, Y.; Chen, Z.; Zhang, P.; Chen, L.; Song, G.; Alharbi, N.S.; et al. Impact of metal ions and organic ligands on uranium removal properties by zeolitic imidazolate framework materials. *J. Clean. Prod.* **2021**, *278*, 123216. [[CrossRef](#)]

55. Liu, Y.; Pang, H.; Wang, X.; Yu, S.; Chen, Z.; Zhang, P.; Chen, L.; Song, G.; Saleh Alharbi, N.; Omar Rabah, S.; et al. Zeolitic imidazolate framework-based nanomaterials for the capture of heavy metal ions and radionuclides: A review. *Chem. Eng. J.* **2021**, *406*, 127139. [[CrossRef](#)]
56. Chai, C.; Gao, J.; Zhao, G.; Li, L.; Tang, Y.; Wu, C.; Wan, C. In-situ synthesis of ultrasmall Au nanoparticles on bimetallic metal-organic framework with enhanced electrochemical activity for estrone sensing. *Anal. Chim. Acta* **2021**, *1152*, 338242. [[CrossRef](#)]
57. Yang, X.; Chen, J.; Liu, H.; Li, X.; Zhong, S. Molecularly imprinted polymers based on zeolite imidazolate framework-8 for selective removal of 2,4-dichlorophenoxyacetic acid. *Colloids Surf. A Physicochem. Eng. Asp.* **2019**, *570*, 244–250. [[CrossRef](#)]
58. Park, K.S.; Ni, Z.; Cote, A.P.; Choi, J.Y.; Huang, R.; Uribe-Romo, F.J.; Chae, H.K.; O’Keeffe, M.; Yaghi, O.M. Exceptional chemical and thermal stability of zeolitic imidazolate frameworks. *Proc. Natl. Acad. Sci. USA* **2006**, *103*, 10186–10191. [[CrossRef](#)]
59. Xiao, T.; Liu, D. Progress in the synthesis, properties and applications of ZIF-7 and its derivatives. *Mater. Today Energy* **2019**, *14*, 100357. [[CrossRef](#)]
60. Cai, W.; Lee, T.; Lee, M.; Cho, W.; Han, D.Y.; Choi, N.; Yip, A.C.; Choi, J. Thermal structural transitions and carbon dioxide adsorption properties of zeolitic imidazolate framework-7 (ZIF-7). *J. Am. Chem. Soc.* **2014**, *136*, 7961–7971. [[CrossRef](#)]
61. Li, Y.; Xu, W.; Zhao, X.; Huang, Y.; Kang, J.; Qi, Q.; Zhong, C. Electrochemical sensors based on molecularly imprinted polymers on Fe<sub>3</sub>O<sub>4</sub>/graphene modified by gold nanoparticles for highly selective and sensitive detection of trace ractopamine in water. *Analyst* **2018**, *143*, 5094–5102. [[CrossRef](#)] [[PubMed](#)]
62. Li, Y.; Li, X.; Chu, J.; Dong, C.; Qi, J.; Yuan, Y. Synthesis of core-shell magnetic molecular imprinted polymer by the surface RAFT polymerization for the fast and selective removal of endocrine disrupting chemicals from aqueous solutions. *Environ. Pollut.* **2010**, *158*, 2317–2323. [[CrossRef](#)]
63. Li, Y.; Zhao, X.; Li, P.; Huang, Y.; Wang, J.; Zhang, J. Highly sensitive Fe<sub>3</sub>O<sub>4</sub> nanobeads/graphene-based molecularly imprinted electrochemical sensor for 17beta-estradiol in water. *Anal. Chim. Acta* **2015**, *884*, 106–113. [[CrossRef](#)] [[PubMed](#)]
64. Thomsen, C.; Reich, S. Doable resonant Raman scattering in graphite. *Phys. Rev. Lett.* **2000**, *85*, 5214–5217. [[CrossRef](#)] [[PubMed](#)]
65. Choi, W.S.; Choi, S.-H.; Hong, B.; Lim, D.-G.; Yang, K.-J.; Lee, J.-H. Effect of hydrogen plasma pretreatment on growth of carbon nanotubes by MPECVD. *Mater. Sci. Eng. C* **2006**, *26*, 1211–1214. [[CrossRef](#)]
66. Kudin, K.N.; Ozbas, B.; Schniepp, H.C.; Prud’homme, R.K.; Aksay, I.A.; Car, R. Raman spectra of graphite oxide and functionalized graphene sheets. *Nano Lett.* **2008**, *8*, 36–41. [[CrossRef](#)]
67. Li, Y.; Li, X.; Dong, C.; Li, Y.; Jin, P.; Qi, J. Selective recognition and removal of chlorophenols from aqueous solution using molecularly imprinted polymer prepared by reversible addition-fragmentation chain transfer polymerization. *Biosens. Bioelectron.* **2009**, *25*, 306–312. [[CrossRef](#)]

**Disclaimer/Publisher’s Note:** The statements, opinions and data contained in all publications are solely those of the individual author(s) and contributor(s) and not of MDPI and/or the editor(s). MDPI and/or the editor(s) disclaim responsibility for any injury to people or property resulting from any ideas, methods, instructions or products referred to in the content.